



# Experimental study of the parameters for stable drop-on-demand inkjet performance

Cite as: Phys. Fluids **31**, 032004 (2019); <https://doi.org/10.1063/1.5085868>

Submitted: 16 December 2018 • Accepted: 20 February 2019 • Published Online: 11 March 2019

 Yuanyuan Liu and  Brian Derby



View Online



Export Citation



CrossMark

## ARTICLES YOU MAY BE INTERESTED IN

[Analysis of drop-on-demand piezo inkjet performance](#)

Physics of Fluids **32**, 022007 (2020); <https://doi.org/10.1063/1.5142023>

[An experimental study of drop-on-demand drop formation](#)

Physics of Fluids **18**, 072102 (2006); <https://doi.org/10.1063/1.2217929>

[Ink-jet delivery of particle suspensions by piezoelectric droplet ejectors](#)

Journal of Applied Physics **97**, 094903 (2005); <https://doi.org/10.1063/1.1888026>

APL Machine Learning

Open, quality research for the networking communities

**Now Open for Submissions**

LEARN MORE

AIP  
Publishing

# Experimental study of the parameters for stable drop-on-demand inkjet performance

Cite as: Phys. Fluids 31, 032004 (2019); doi: 10.1063/1.5085868  
Submitted: 16 December 2018 • Accepted: 20 February 2019 •  
Published Online: 11 March 2019



Yuanyuan Liu<sup>1,2,3</sup>  and Brian Derby<sup>1,2,a)</sup> 

## AFFILIATIONS

<sup>1</sup>Beijing Advanced Innovation Center for Biomedical Engineering, Beihang University, Beijing 100083, China

<sup>2</sup>School of Materials, University of Manchester, Manchester M13 9PL, United Kingdom

<sup>3</sup>Key Laboratory for Biomechanics and Mechanobiology of Ministry of Education, School of Biological Science and Medical Engineering, Beihang University, Beijing 100083, China

<sup>a)</sup> Author to whom correspondence should be addressed: [brian.derby@manchester.ac.uk](mailto:brian.derby@manchester.ac.uk)

## ABSTRACT

We present an experimental study of drop-on-demand inkjet behavior, with particular emphasis on the thresholds for drop generation and formation of satellite drops, using inks covering a range of fluid properties. Drop behavior can be represented as a “phase diagram” in a parameter space bound by the dimensionless number  $Z$  (the inverse of the Ohnesorge number) and the Weber number of the fluid jet prior to drop formation,  $We_j$ . Stable drop generation is found to be bounded by a parallelogram with minimum and maximum values of  $2 < We_j < 25$ . The lower bound indicates where capillary forces prevent drop ejection, and the upper bound indicates the onset of satellite drop formation. For  $Z < 50$ , the critical  $We_j$  for drop ejection increases with decreasing  $Z$  because of the contribution of viscous dissipation during drop formation. This requires an increase in the voltage required to drive the piezoelectric actuator until at  $Z \approx 0.3$  no drop ejection is possible. With  $Z > 4$ , the value of  $We_j$  at which satellite drops form decreases with increasing  $Z$  until at very large values of  $Z$  single drops can no longer form at any  $We_j$ . However, despite the large range of fluid properties over which stable drops can form, the need for a large range of both  $Z$  and  $We_j$  limits the region of practical ink design to the approximate range of  $2 < Z < 20$ . These results are shown to be compatible with current models of the drop formation process reported in the literature.

© 2019 Author(s). All article content, except where otherwise noted, is licensed under a Creative Commons Attribution (CC BY) license (<http://creativecommons.org/licenses/by/4.0/>). <https://doi.org/10.1063/1.5085868>

## I. INTRODUCTION

Inkjet printing has applications beyond the graphic arts in diverse areas such as printed electronics,<sup>1,2</sup> printed ceramics,<sup>3–5</sup> and biomaterials.<sup>6</sup> These all require the formation and deposition of droplets in a controlled manner, with droplets traveling at a stable velocity and with a precise and defined volume, typically in the range of 1–100 pl ( $10^{-15}$ – $10^{-13}$  m<sup>3</sup>). The increased application area of the technology has required the development of an extensive array of inks of a range of chemistries and potential rheological properties, including polymer solutions,<sup>7</sup> nanoparticle suspensions,<sup>3</sup> and suspensions of high aspect ratio particles including nanotubes<sup>8</sup> and atomic thick layers of two-dimensional (2D) materials.<sup>9,10</sup> There are a large number of operating modes by which inkjet printers may generate droplets, and the principles of these have been reviewed elsewhere.<sup>11–13</sup> However, most applications

outside marking, coding, and low-resolution graphics use piezoelectric actuated drop-on-demand (DOD) inkjet printing, and hence this study is limited to the formation of droplets from inks delivered by this method.

There has been significant previous study of the influence of ink rheological properties on DOD inkjet printability. Dijkstra and Fromm carried out the earliest work focused on understanding the influence of fluid physical properties on the mechanisms of drop generation during inkjet printing.<sup>14,15</sup> Fromm used a velocity independent dimensionless number  $Z$  (the inverse of the Ohnesorge number) in his calculations,

$$Z = \frac{1}{Oh} = \frac{Re}{\sqrt{We}} = \frac{\sqrt{\gamma\rho a}}{\eta}, \quad (1)$$

where  $Oh$ ,  $Re$ , and  $We$  are the Ohnesorge, Reynolds, and Weber numbers, respectively;  $\gamma$ ,  $\rho$ , and  $\eta$  are the surface tension, density,

and dynamic viscosity of the fluid, respectively; and  $a$  is the characteristic length, here taken as the diameter of the printer orifice. Such a fluid velocity independent dimensionless number has advantages as a suitable metric for fluid selection. Fromm suggested that  $Z > 2$  for stable drop formation because viscous dissipation prevents drop ejection at lower values. Reis and Derby proposed, on the basis of computational fluid dynamics (CFD) modeling, that  $Z$  should be in the range  $1 < Z < 10$ , with viscous dissipation preventing drop ejection when  $Z < 1$ , while satellite drops were predicted to form together with the primary drop when  $Z > 10$ .<sup>16</sup>

The principles of drop formation indicate that a minimum fluid velocity must be achieved by the actuating pulse to overcome viscous and surface tension forces during drop formation. Initial simple models by Duineveld *et al.*<sup>17</sup> proposed that the minimum velocity was determined by the inertial force required to overcome surface energy, in which case the minimum fluid velocity is defined by a minimum Weber number, with  $We > 1$  for drop generation. Xu and Basaran carried out a numerical simulation of drop formation and found that at  $Z = 10$ ,  $We > 10$  for stable drop formation.<sup>18</sup> However, another numerical study by Mao *et al.*<sup>19</sup> reported minimum velocities in line with the prediction of Duineveld *et al.*

An upper bound for printability is normally taken as the critical velocity for the onset of satellite drop formation in addition to the leading printed droplet. During DOD inkjet printing, the actuation pulse drives a column of fluid through the printer orifice. Ideally, once the pulse terminates, the column thins rapidly to a thread and pinches off leading to a characteristic drop with an elongated tail that retracts to form a single spherical drop in flight; satellite drops form if there is more than one pinch point in the tail. Dong *et al.* studied DOD inkjet drop formation using three fluids, water, a water-glycerol solution, and a water-glycerol-isopropanol solutions with  $Z = 44$ , 8.9, and 6.2, respectively, and a range of actuation voltages.<sup>20</sup> In all three cases, the length of the liquid column ejected increased with increasing actuation voltage. At all actuation voltages, water formed satellite drops with the number of satellites increasing with actuation voltage, and the authors suggested that the breakup of the liquid thread was through the propagation of capillary waves. The glycerol solutions showed more stable liquid threads, which either retracted back into the leading drop or, at long lengths when a single pinch off occurred, formed a satellite that eventually recombined with the leading drop. This is consistent with the work of Notz and Basaran,<sup>21</sup> who modelled the stability of isolated liquid filaments and found that when  $Z < 10$  filaments retract to a sphere, whereas at larger values they pinch off satellites.

This brief review suggests that the principal mechanisms for drop formation during DOD inkjet printing are relatively well understood; however, this is not the case. The majority of the experimental studies for DOD inkjet printing have used simple tubular actuator droplet generators and similar ranges of experimental fluids. Despite this, they report different limiting values for  $Z$  defining the range of fluid printability with  $1.5 < Z < 12.7$ ,<sup>16</sup>  $4 < Z < 14$ ,<sup>22</sup> and  $1 < Z < 16$ .<sup>5</sup> Although there is general agreement that the minimum value of  $Z$  is close to 1, the upper bounding value shows greater variation. Indeed there are a number of reports of successful DOD inkjet printing with  $Z \gg 10$ .<sup>7,23-25</sup> See Table III in the Appendix for a full

review of the published data. The general trend of these observations has been confirmed by numerical modeling of the drop formation process.<sup>18,19,26,27</sup> However, the various models presented for DOD inkjet drop formation do not use common or consistent boundary conditions defining the initial fluid flow. This neither allows easy comparison between models and experiments nor between different modeling approaches, especially given that experimental studies have demonstrated that the velocity and ejected volume of a piezoelectric DOD inkjet droplet can be controlled within a certain range by appropriate design of the actuation pulse (e.g., pulse shape, voltage, frequency).<sup>4,24,28</sup> Thus we believe there is a need for further careful experimental study of the interrelation between ink physical properties and fluid actuation during the drop formation process.

Here we present a study of the drop formation mechanisms as a function of fluid properties and actuation pulse using a print-head from a commercial inkjet printing system (Dimatix Material Printer, Fujifilm Dimatix, Santa Clara, CA, USA). This generates droplets through the shear mode actuation of the wall of a fluid filled chamber. We have selected this for two reasons. First it is the printing system of choice in a very large number of reports in the literature for the printing of functional materials, e.g., for printed electronics, sensors, and displays; thus reports of printability and ink design using this equipment will be of wide ranging interest. Second, we wish to compare our experimental dataset with those from other authors in the literature who have mostly used drop generators actuated by the contraction of a tubular fluid reservoir is changed,<sup>18,19,26,27</sup> to determine whether there is any strong influence of actuator design on DOD inkjet drop generation.

## II. EXPERIMENTAL PROCEDURE

To investigate the influence of fluid properties on ink printability, 11 solution based inks were prepared with compositions selected to obtain a range of  $Z$  from 0.05 to 36.8. Ink formulations included de-ionized (DI) water, solutions of DI water and ethylene glycol, pure ethylene glycol (Sigma-Aldrich, Gillingham, Dorset, UK), pure diethylene glycol (Sigma-Aldrich), and pure glycerol (Sigma-Aldrich). Inks were either used in pure form or mixed to the desired composition in glass laboratory vessels. The inks were filtered through a  $0.45 \mu\text{m}$  polytetrafluoroethylene (PTFE) syringe filter (Puradisc Whatman, Little Chalfont, UK). 4 ml aliquots of the inks were extracted using a 5 ml adjustable-volume pipette (Fisher Scientific Ltd., Loughborough, UK) and weighed using a laboratory balance (ATX, Marsden Weighing Machine Group Ltd., Rotherham, UK). The mean densities of the inks were calculated from the measured volumes and weights. Viscosity and surface tension were measured using a single head Hybrid Rheometer (Discovery Hybrid Rheometer, TA Instruments, Inc., New Castle, DE, USA) and a Drop Shape Analyser (DSA 100, Krüss GmbH., Hamburg, Germany), respectively. The physical properties of the inks and the dimensionless constant  $Z$  are displayed in Table I.

All inks were used with a shear mode actuated drop generator with nozzle diameter  $21.5 \mu\text{m}$  that produces drops of nominal volume 10 pl (DMC-11610, Fujifilm Dimatix, Santa Clara). This was mounted on a PiXDRO LP50 inkjet printer (Meyer and Burger,

**TABLE I.** Composition and fluid physical properties of the inks, together with the computed value of the dimensionless number  $Z$ , taking the characteristic length to be the diameter of the printing orifice ( $21.5 \mu\text{m}$ ).

Ink no.	Composition	Density ( $\text{kg m}^{-3}$ )	Dynamic viscosity (mPa s)	Surface tension ( $\text{mN m}^{-1}$ )	$Z$
1	De-ionized (DI) water	991	1.07	72.7	36.8
2	EG(0.05):Water(0.95)	992	1.16	69.5	33.2
3	EG(0.10):Water(0.90)	994	1.47	68.9	26.1
4	EG(0.15):Water(0.85)	1002	2.32	67.7	16.5
5	EG(0.25):Water(0.75)	1014	2.72	67.0	14.1
6	EG(0.50):Water(0.50)	1048	4.39	60.3	8.40
7	EG(0.75):Water(0.25)	1077	7.81	52.7	4.47
8	EG(0.85):Water(0.15)	1093	10.5	50.2	3.28
9	Ethylene glycol (EG)	1105	15.8	45.5	2.08
10	Diethylene glycol	1090	27.1	42.7	1.17
11	Glycerol	1261	934.0	76.2	0.05

Eindhoven, Netherlands) equipped with a high-speed camera system and a flash light-emitting diode (LED) for the stroboscopic imaging of printed droplets. The drop generator was actuated using a unipolar trapezoidal waveform of peak amplitude in the range 10–40 V, with rise, dwell, and fall times of  $1 \mu\text{s}$ ,  $3 \mu\text{s}$ , and  $3 \mu\text{s}$ , respectively (Fig. 1). Note the minor secondary peak that cannot be avoided in the actuation software used with the DMC11610, and it is believed that this has an amplitude too small to influence the jetting characteristics.

Drop velocities and volumes were calculated from stroboscopic images. The PiXDRO-LP50 is equipped with proprietary image analysis software (Dropview) allowing image capture of individual droplets and can be used to calculate the droplet volumes, positions, travel angles, and travel velocities. The mean drop velocity was calculated by measuring the distance travelled between LED trigger delays of  $60 \mu\text{s}$  and  $120 \mu\text{s}$ . The inks were all printed at a jetting frequency of 1 kHz. Drop images were captured by increasing the

delay time of the camera from  $0 \mu\text{s}$  in steps of  $10 \mu\text{s}$  until the droplet disappears from the screen.

### III. RESULTS

The influence of the dimensionless number  $Z$  on drop behavior is presented in Fig. 2, which shows a sequence of stroboscopic images of drop formation using inks 1–9, spanning a range of  $Z$  from 2 to 37. The drops were formed using identical actuation pulses with a dwell amplitude of 23 V. Each sequence of images is taken with a  $10 \mu\text{s}$  delay increment; hence, the distance travelled between each image is proportional to drop velocity, which increases as  $Z$  rises from 2 to 14 and remains approximately constant after that. Inks 10 and 11, with  $Z = 1.17$  and  $0.05$ , did not eject drops with this actuation signal. At low values of  $Z$ , a single drop is formed, and with  $Z > 14$ , multiple or satellite drops are present. This behavior is consistent with that proposed by Reis and Derby<sup>16</sup> and confirmed by Jang,<sup>22</sup> albeit with slightly different limiting values of  $Z$ .

Figure 3 shows a sequence of stroboscopic images of drop formation using ink 7 ( $Z = 4.47$ ) and varying the amplitude of the actuating pulse in the range 16–30 V. When the voltage is smaller than 16 V, no stable drops were generated. As the actuation voltage increases, the fluid jet can be seen at small strobe time intervals, and at 23 V, the jet is seen to extend from the nozzle attached by a thin ligament of fluid, which ruptures to release a single drop. As the voltage is increased to 25 V, the ligament ruptures near the nozzle and the resulting tail retracts through surface tension into the drop within  $100 \mu\text{s}$ . With larger voltages, longer tails and larger drop volumes form and the ligament ruptures both near the nozzle and the leading drop to form first a single satellite drop and then multiple satellites. At intermediate actuating voltages, the satellite catches up with the main drop and is reabsorbed. However, when the amplitude  $> 28$  V, a number of stable satellites trail the primary leading drop, and as the pulse voltage is further increased, additional satellites are formed. There is also a clear increase in the leading drop velocity as

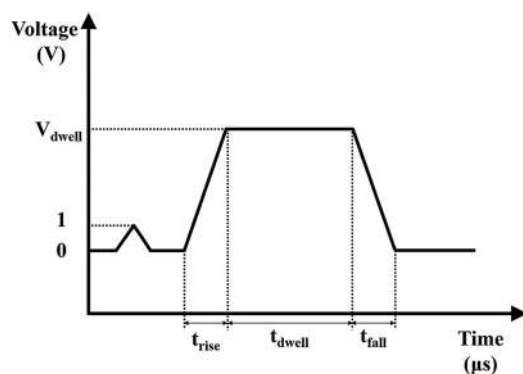


**FIG. 1.** Schematic of the unipolar trapezoidal waveform used with the Fujifilm Dimatix DMC 11610 10 pl droplet generator.

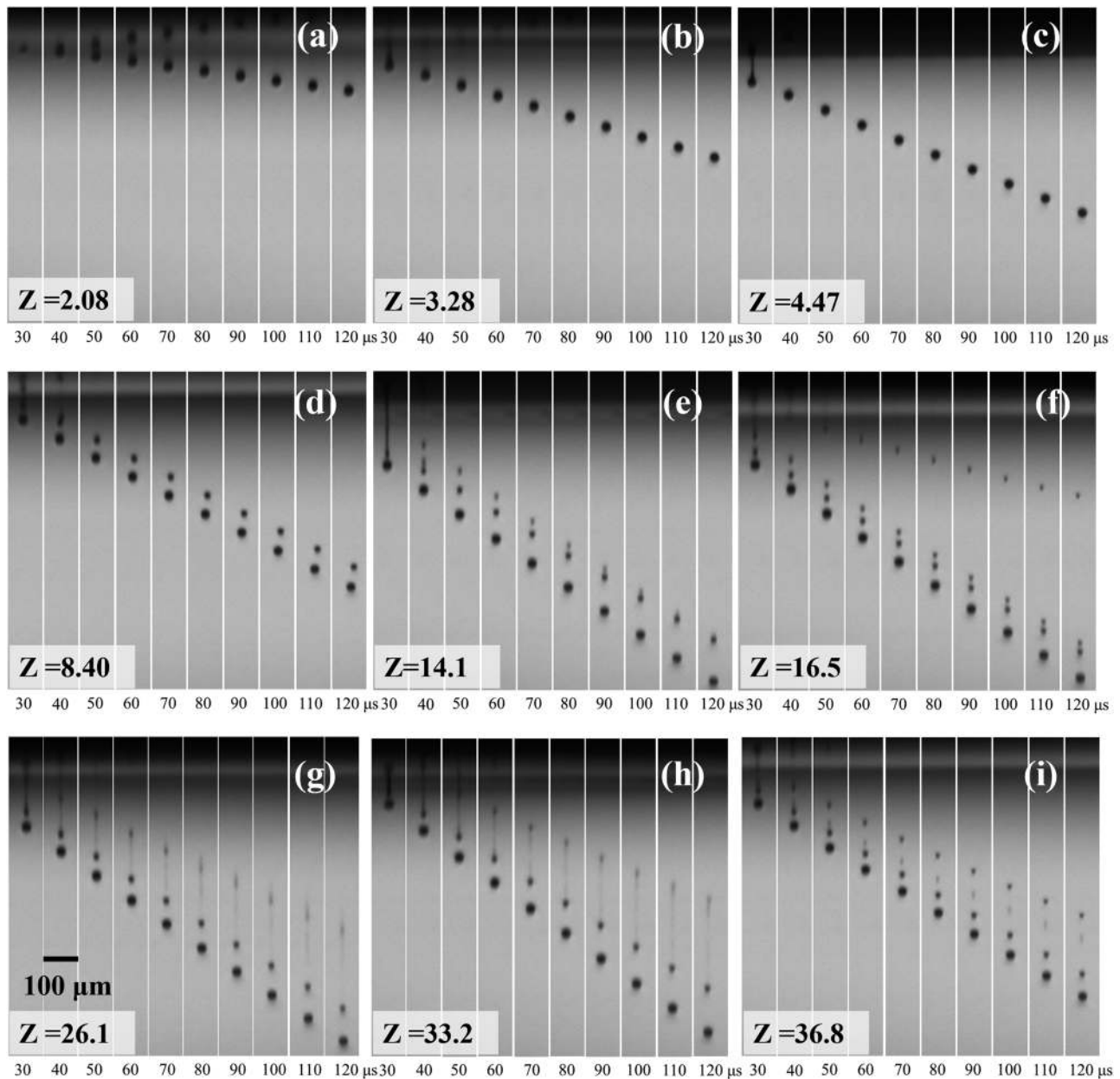


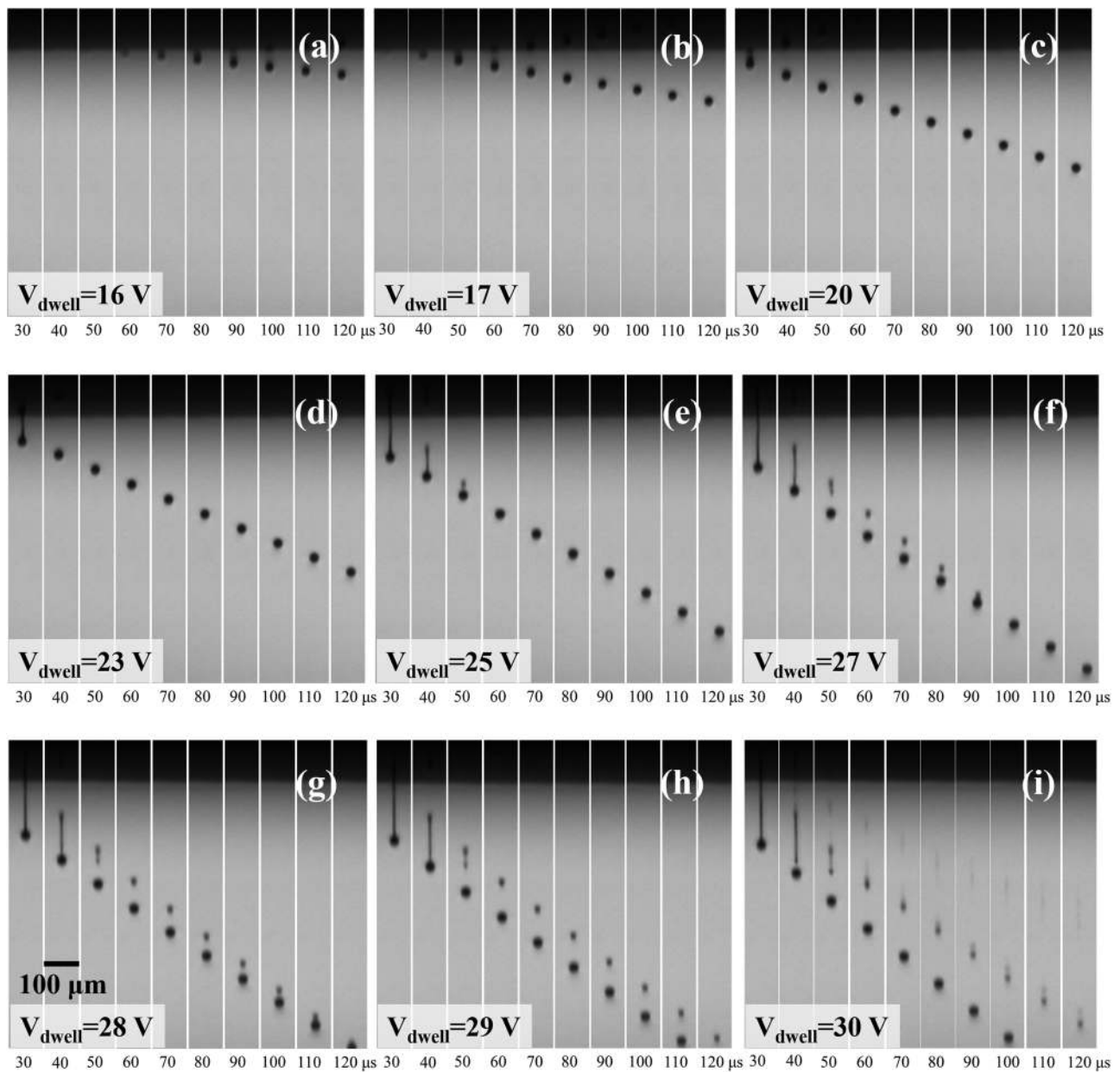
**FIG. 2.** Images of drop formation taken at  $10 \mu\text{s}$  increments of strobe delay for inks with  $Z$  ranging from 2 to 37 at a constant dwell voltage of 23 V using a 10 pl DMC-11610 drop generator. (a) Ink 9,  $Z = 2.08$ ; (b) ink 8,  $Z = 3.28$ ; (c) ink 7,  $Z = 4.47$ ; (d) ink 6,  $Z = 8.40$ ; (e) ink 5,  $Z = 14.1$ ; (f) ink 4,  $Z = 16.5$ ; (g) ink 3,  $Z = 26.1$ ; (h) ink 2,  $Z = 33.2$ ; (i) ink 1,  $Z = 36.8$ .

the actuating voltage increases. A threshold for satellite formation with increasing drop velocity has also been reported by Tsai<sup>23</sup> and Nallan.<sup>29</sup>

Figures 4(a) and 4(b) show the drop velocity and volume as a function of actuation voltage. In the case of multiple drop ejection, the datum is taken from the leading drop. In all cases, the ejected drop velocity and volume increase with increasing actuation voltage.

This has also been seen with studies using cylindrical actuators.<sup>4,28</sup> Note that the drop velocity as a function of actuating pulse amplitude follows a similar trend for each fluid but above a critical or threshold voltage for drop ejection that increases as  $Z$  decreases. If we replot the velocity data as a function of the voltage difference,  $\Delta V$ , between the actuating voltage and the critical threshold for drop ejection [Fig. 4(c)], there appears to be a linear universal relation

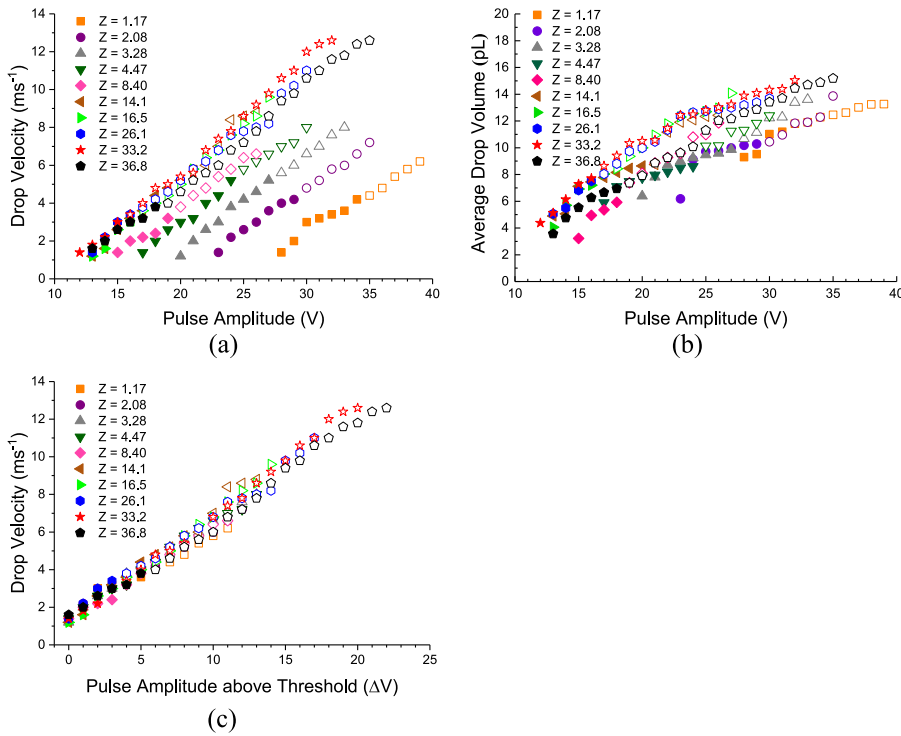




**FIG. 3.** Images of drop formation from ink 7 ( $Z = 4.47$ ) taken at  $10 \mu\text{s}$  increments of strobe delay, with actuation amplitudes of (a) 16 V, (b) 17 V, (c) 20 V, (d) 23 V, (e) 25 V, (f) 27 V, (g) 28 V, (h) 29 V, (i) 30 V.

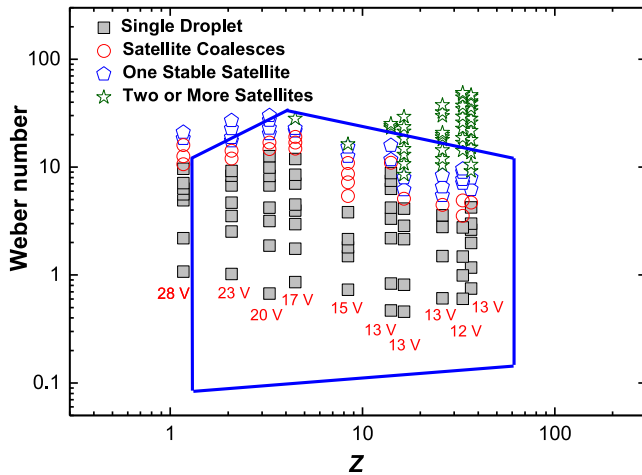
between drop velocity and  $\Delta V$ . The relation between drop volume and actuating voltage shows a similar trend for each ink tested, but the data are not coincident nor are they if plotted against  $\Delta V$ . At a given actuation voltage, the volume ejected increases slightly with increasing  $Z$ . A similar monotonic relation between drop volume and actuating voltage has been reported previously with cylindrical actuators and also the relationship between ejected drop volume and  $Z$ .<sup>28</sup>

Figure 5 summarizes the range of drop formation morphologies observed with all the fluids and pulse actuation voltages, with the drop velocity represented in dimensionless form as the Weber number,  $We$ . Each fluid is presented as a column of data points at constant  $Z$ , with each data point representing drop behavior at 1 V increments of the actuating voltage above the critical value for drop ejection. Four classes of drop behavior are seen: filled square symbols indicate the ejection of a stable single drop; circles indicate the



**FIG. 4.** Influence of actuating voltage on ejected drop properties. Individual fluids and values of  $Z$  are indicated; filled symbols indicate a single drop, and open symbols two or more drops formed. (a) Leading drop velocity as a function of actuating pulse voltage. (b) Leading drop volume as a function of actuating pulse voltage. (c) Drop velocity as a function of actuating voltage above the threshold for drop ejection.

formation of a single satellite droplet of greater velocity than the leading droplet such that they recombine in flight within 1 mm of the nozzle (the limit of the field of view of our imaging system);



**FIG. 5.** Influence of fluid physical properties, characterized by  $Z = 1/Oh$ , and actuation voltage on dimensionless drop velocity (Weber number) and morphology. Filled square symbol represents a single drop, circle represents a satellite that merges with the leading drop in flight, pentagon represents a single stable satellite, and star represents two or more satellites. Minimum voltage for drop ejection is indicated for each fluid with subsequent data points increasing by 1 V with increasing  $We$ . The blue lines indicate the region of stable drop formation reported by Nallan *et al.*<sup>29</sup>

pentagons indicate the presence of a single stable satellite droplet with velocity less than or equal to the leading drop; and finally a five-pointed star indicates the presence of multiple satellites. Superimposed on this figure is a five sided polygon that identifies the region of printability reported by Nallan *et al.*, who used a tubular actuated drop generator to study drop formation using a similar range of inks.<sup>29</sup> The bounding values of  $Z$  are similar to our findings, but single drops were reported for lower values of  $We$ , and the transition to satellites occurred at a slightly higher value than reported here. Nonetheless, this comparison of our data with the results of Nallan *et al.* suggests that inkjet drop behavior is only slightly influenced by the method of actuation.

**IV. DISCUSSION**

**A. Minimum voltage for drop ejection**

Duineveld *et al.* suggested that the minimum velocity for drop ejection is controlled by the inertial force required to overcome the formation of the drop surface area,<sup>17</sup> and this has been supported by the numerical models of Xu and Basaran.<sup>18</sup> However, in addition to the formation of a new surface, there are other dissipative processes causing the ejected drop velocity,  $v_d$ , to be smaller than the fluid jet velocity,  $v_j$ , in the drop generator prior to drop formation and detachment. Driessen and Jeurissen produced a model to predict the change in velocity of a printed drop by considering drop formation as a momentum balance between advection, the increase in surface area to form a drop, and viscous dissipation during the retraction of the liquid ligament that accompanies the drop.<sup>30</sup>

Here we provide a concise summary of the approach used by Driessen and Jeurissen, but for a full derivation, we refer to the original work.<sup>30</sup> Their model uses an approach similar to that first used by Dijkstra<sup>15</sup> but using a momentum balance rather than an energy balance. The volume of the ejected drop,  $V_d$ , is defined by the integral of the fluid flow rate through the nozzle, taken as a circular section with radius  $r$ , with

$$V_d = \int_{t_o}^{t_e} \pi r^2 v_j dt. \quad (2)$$

In Eq. (2),  $t_o$  and  $t_e$  are the time at which fluid flows toward the nozzle to form the initial jet and the time when the flow arrests or reverses. The two processes that reduce the momentum of the fluid advection are viscous dissipation during the formation and shrinking of the fluid neck as a droplet separates from the fluid jet and the formation of the detached drop surface area. The momentum transfer,  $p_n$ , during neck formation and thinning occurs during the viscous processes accompanying neck stretching and thinning, assuming that the initial neck radius is identical to the nozzle radius, is given by

$$p_n = -3\pi r^2 \eta. \quad (3)$$

The final contribution is from the capillary force opposing the fluid as it leaves the nozzle. This is controlled by the nozzle radius, and the resulting momentum change is

$$p_c = -(t_o - t_e) \pi r \gamma. \quad (4)$$

Combining the momentum change from advection, viscous dissipation, and capillarity, an approximate expression for the ejected drop velocity is given by

$$v_d = \frac{1}{\rho V_d} \left( \int_{t_o}^{t_e} \rho \pi r^2 v_j^2 dt - 3\eta \pi r^2 - (t_e - t_o) \pi r \gamma \right). \quad (5)$$

In the absence of viscous dissipation, and assuming the fluid flow is modelled as a fixed period at constant velocity,  $v_d$  will be negative if  $\rho r v_j^2 < \gamma$ , or  $We < 2$  (here we use the diameter as the characteristic length), which is identical to the prediction of Duineveld *et al.*<sup>17</sup> It is not possible to measure  $v_j$  directly because of the limitations of the optics of our system; thus, Eq. (5) is used to estimate the fluid jet velocity from our measurements of drop velocity and drop volume.

If the fluid flow in the tube is simplified to a constant velocity for a time,  $\delta t = t_o - t_e$ , the volume of the ejected drop is given by  $V_d = \pi r^2 v_j \delta t$ , and Eq. (2) can be rearranged to give

$$v_j^2 - v_j v_d - \frac{3\eta}{\rho \delta t} - \frac{\gamma}{\rho r} = 0. \quad (6)$$

This can be solved analytically to obtain  $v_j$  for a given  $v_d$ , with the only unknown being the time,  $\delta t$ , for the fluid flow in the actuator. Considering that the actuating pulse in Fig. 1 has a rise time of 3  $\mu$ s and a total duration of 7  $\mu$ s, it is reasonable to expect the value of  $\delta t$  to lie somewhere in this range. In order to determine  $\delta t$ , we compare the predicted drop volume,  $V_d = \pi r^2 v_j \delta t$ , with that determined experimentally for all values of  $Z$  and actuating voltages. The optimum value of  $\delta t$  was found to be 3.9  $\mu$ s. Thus we are able to estimate the fluid jet velocity at the onset of drop formation, and this is displayed in Table II.

**TABLE II.** Minimum drop velocity for drop ejection,  $v_{min}$ , equivalent estimated fluid jet velocity,  $v_{jmin}$ , and the minimum Weber number of the fluid jet  $We_{jmin}$ .

Ink no.	$Z$	Threshold voltage (V)	$v_{min}$ (ms <sup>-1</sup> )	$v_{jmin}$ (ms <sup>-1</sup> )	$We_{jmin}$
1	36.8	13	1.6	3.7	4.0
2	33.2	12	1.4	3.5	3.8
3	26.1	13	1.4	3.5	3.9
4	16.5	13	1.2	3.5	3.9
5	14.1	13	1.2	3.5	4.1
6	8.40	15	1.4	3.7	5.2
7	4.47	17	1.4	4.0	6.9
8	3.28	20	1.2	4.1	7.7
9	2.08	23	1.4	4.6	11.1
10	1.17	28	0.4	5.0	13.6
11	0.05	...	...	...	...

From the results in Table II, we see that for inks 1–5, with  $Z > 14$ , the surface tension term dominates and there is a constant critical  $We_j$  that must be exceeded for drop formation. Inks 6–10 have lower values of  $Z$ , and here viscous dissipation processes during thread extension and rupture become increasingly more important and the minimum jet velocity for drop ejection increases. Thus the observed minimum or threshold actuating voltage for drop ejection is better considered as a minimum fluid jet velocity (and thus  $We_j$ ) for drop ejection. Unfortunately it is not possible to compare our results with the drop generation threshold data published by Nallan *et al.*<sup>29</sup> because they do not report the ejected drop volume and hence the fluid jet velocity cannot be estimated from their drop velocity data.

### B. Threshold for satellite drop formation

Figure 5 shows that the threshold for satellite formation is also a function of  $Z$ . At low  $Z$ , there appears to be a critical value of  $We \approx 10$  above which stable satellites form. However, when  $Z > 6$ , the maximum  $We_j$  before satellites form reduces rapidly to around a value of 4 at the largest values of  $Z$  explored in this study. Figure 5 also shows the limiting values for stable drop ejection reported by Nallan *et al.* using a different drop generator design.<sup>29</sup> In Nallan's study, there is also a decrease in the critical  $We$  at larger values of  $Z$  and a clear maximum value of  $We$  at  $Z \approx 5$ , roughly where we see the onset of the decrease in critical  $We$ . The prior work of Nallan did not consider the transition from single to multiple drop ejection in detail. Here we identified three drop ejection regimes as the drop Weber number increases:

- (i) An isolated stable drop.
- (ii) The drop accompanied by a single satellite, which may have a greater velocity than the leading drop and after a brief time interval coalesces to form a single drop or a velocity equal to or lower than the leading drop and remain as a satellite to the leading drop.
- (iii) The drop accompanied by multiple satellites.



At low values of  $Z$ , satellites were rarely seen; however, the maximum drop velocity at low  $Z$  was limited by the actuation of the drop ejector, and it is possible that multiple satellites may form at larger drop velocities than available to this study. Inks 1–7 (with  $Z > 4$ ) all showed all 3 regimes of drop behavior. However, although there is some evidence for a decrease in  $We$  at the transitions from regimes (i)–(ii)–(iii) that can be seen with increasing  $Z$  in Fig. 5, there is little correlation or trend that can be inferred from the results other than a wider range of  $We$  for multiple drop formation as  $Z$  increases.

Satellite formation is associated with the stability of the fluid ligament that forms during drop ejection and pinch-off. An early study of Schulkes considered the stability of a free standing liquid filament and demonstrated that viscous filaments could retract to form a sphere, even if their aspect ratio was such that a Rayleigh-Plateau instability was expected.<sup>32</sup> In such cases, the viscosity damps the capillary undulations and there is sufficient time for the filament to retract. This behavior was shown to be dependent on the Ohnesorge number with stable contraction predicted if it exceeded a value in the range  $10^{-2}$ – $10^{-1}$  ( $Z < 10$ – $100$ ) with the transition also dependent on the length of the fluid ligament. This and similar work was reviewed by Notz and Basaran,<sup>21</sup> who carried out further numerical simulation of fluid ligament stability to predict the interrelation between fluid properties, ligament length, and the onset of ligament instability. They found that for  $Z < 10$  ligaments were stable irrespective of length and always retracted to form a stable drop, and at higher values of  $Z$ , ligament stability also required the ligament to be smaller than a critical aspect ratio of 27.5 when  $Z = 20$  and reducing to 5.5 when  $Z = 1000$ .

Kim and Baek carried out an extensive exploration of the parameter space for DOD inkjet printing using a numerical model.<sup>33</sup> They too found a transition in behavior at a value of  $Z \approx 10$ , with multiple satellite drops forming above a critical  $We$  at high  $Z$  and a small single satellite forming at low  $Z$ . Our data are consistent with a change in satellite drop behavior at an intermediate value of  $Z \approx 10$ , and we found that satellite drops always formed above a critical drop/jet Weber number but that multiple satellite drops were only seen at high  $Z$ . Kim and Baek predicted that at low  $Z$  the single satellite drop is accompanied by a thin liquid thread, a phenomenon that we have not seen although it is possible that they cannot be resolved with our imaging system. Dong *et al.* reported a study of drop formation using a push mode DOD inkjet drop generator and considered the dynamics of ligament breakup into satellite drops.<sup>20</sup> They found that the rate of ligament break up was a function of  $Oh$ , with the critical length of stable liquid filament increasing with increasing  $Oh$ , i.e., with decreasing values of  $Z$ .

It is important to note that satellite drop formation is an aspect of the breakup of the fluid ligament that forms behind the drop. It is well known that this can depend on the actuating waveform in DOD inkjet printing; thus, this aspect of the study is not complete.<sup>34</sup>

### C. Printability phase diagram

Printability phase diagrams within a parameter space defined by fluid property dimensionless numbers have been proposed

earlier. Derby and Reis<sup>31</sup> used axes of  $Re$  and  $We$  and proposed a printability range delimited by lines  $1 < Z < 10$ , a maximum drop velocity determined by a splashing transition, and a minimum  $We$  as proposed by Duineveld *et al.*<sup>17</sup> This was further elaborated in later publications.<sup>5,12</sup> Kim and Baek defined a printability phase diagram using computational fluid dynamics (CFD) modeling with axes of  $We$  and the Capillary number,  $Ca = \eta v/\gamma$ ,<sup>33</sup> and this was in part verified by the experimental study of Nallan *et al.*<sup>29</sup> However, phase diagrams plotted from experimental data have generally used the velocity of the printed drop in flight as the characteristic velocity in the dimensionless parameters used to define the appropriate parameter space. We contend that this is not appropriate for considering the conditions for drop generation because, self-evidently, the lower limit for drop generation is defined by a velocity of zero. Thus we propose that a more appropriate dimensionless number to define fluid velocity is the Weber number of the fluid in the nozzle or jet prior to the drop formation process,  $We_j$ . Here we propose a printability phase space with axes of  $Z$  (alternatively  $Oh$ , its inverse) and  $We_j$ . The parameter  $Z$  is independent of velocity [Eq. (1)] and contains a single non-material parameter, a characteristic dimension of the printing nozzle (in this case taken as its diameter). Hence  $Z$  provides a relatively device independent measure of ink quality, particularly because the diameters of practical printing nozzles span a relatively small range.

Figure 6 shows our data plotted in  $Z$ – $We_j$  space, where we have determined  $We_j$  using the estimated jet velocity,  $v_j$ , calculated by solving Eq. (6) for each value of the drop velocity,  $v_d$ . Figure 6 provides a more informative analysis of the threshold for drop formation. A notional set of limiting bounds for stable single drop formation is superimposed upon our experimental data in Fig. 6, indicated by bold blue lines in the form of a quadrilateral. The minimum value for  $We_j$  observed here was  $\approx 4$ . However, we do not believe that this

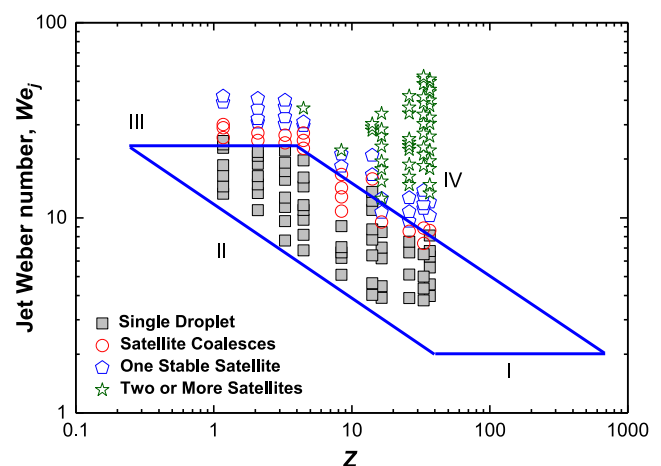


FIG. 6. Phase diagram for printability in a parameter space of  $Z$  and the jet Weber number,  $We_j$ . Filled symbols indicating stable single drop generation at lower values of  $We_j$  and a sequence of satellite drops forming above an upper threshold value of  $We_j$ . Superimposed upon the experimental data is a quadrilateral representing the inferred regime of fluid printability, which indicates 4 transition regimes labeled I–IV.

necessarily represents the bounding value because we only investigated drop formation at 1 V increments of actuation and other work has reported drops with lower velocity in flight than seen in this study, thus a smaller lower bound of  $We_j$  is likely. Here we use the bounding value of  $We_j = 2$ , as proposed by Duineveld *et al.* in an earlier study.<sup>17</sup> Note that this bound is also predicted by Eq. (5), if the effect of fluid viscosity is negligible. Thus the lower horizontal line represents a lower bounding value for drop generation controlled by the surface tension of the jetting fluid (Bound I) evident at larger values of  $Z$ .

A diagonal line (bound II) shows that at lower values of  $Z$  the drop generation threshold requires a greater jet velocity to form and pinch off a drop, as indicated by the increasing critical actuating voltage [Fig. 4(a)]. This line is constructed from our experimental data and is extrapolated to intersect our bounding minimum  $We_j = 2$  at  $Z \approx 40$ . An upper bounding horizontal line at  $We_j \approx 25$  represents a critical  $We_j$  for the formation of satellite drops (bound III). At low values of  $Z$ , this leads to the formation of a single satellite drop. We have no data for drop generation in the regime  $0.05 < Z < 1.17$ , representing the transition between ink 11 (unprintable) and ink 10 (printable); thus, the intersection of the drop formation limit (bound II) with the satellite formation limit of  $We_j = 25$  at  $Z = 0.3$  is an extrapolation. However, from data in the literature (see Table III in the Appendix), there is evidence for printable inks with  $Z < 1$ .

When  $Z > 4$ , the critical  $We_j$  for satellite formation decreases and the generation of multiple satellites is observed (bound IV). This boundary is less easily defined from the experimental data, e.g., inks 5 and 6 ( $Z = 14.1$  and  $8.40$ , respectively) showing satellite formation at, respectively, much higher and lower values of  $We_j$  than would be expected from the trend seen with the sequence of inks. Thus line IV, approximately, defines the region where single drops form, from  $We_j = 25$  at  $Z = 4$  to the intersection of the lower bounding value of  $We_j = 2$  at  $Z = 700$ . Again we justify extending our printability bounds from evidence in the published data that stable drops are possible at  $Z > 100$  under certain conditions (Table III in the Appendix).

Our experimental data and guided extrapolation suggests that there is a very large range of fluids bounded by  $0.3 < Z < 700$  where stable drops are possible. However, for an ink to have utility, we would expect it to be free from satellite drop formation over a large range of drop velocities, and as can be seen from Fig. 6, at both high and low values of  $Z$ , the interval of stable fluid velocity ( $We_j$ ) decreases. In addition, the ejected drops must possess sufficient velocity to travel from the nozzle to the substrate without disturbance, and thus drops generated with low velocity (low values of  $We_d$ ) may not be practical. Thus we propose a smaller limit for useful printability of  $2 < Z < 20$  from our data.

The shape of the printable region inferred from our experiments may also explain the large and disparate limiting range of the bounding values of the parameter  $Z$  reported in a number of studies of ink printability (Table III in the Appendix). If experiments (or simulations) are undertaken using a limited range of drop generation actuation (or jet fluid velocity), only a narrow range of  $We_j$  is probed, and hence behavior is limited by a maximum and minimum  $Z$ . However, another study may interrogate a different range of  $We_j$  and thus sample a regime with a different  $Z_{min}$

and  $Z_{max}$ . At all values of  $We_j$  where stable drops are formed, the limiting values of  $Z_{min}$  and  $Z_{max}$  span approximately an order of magnitude, i.e.,  $Z_{max}/Z_{min} \approx 10$ , which is consistent with earlier studies.<sup>5,16,22</sup>

## V. CONCLUSIONS

The printability of an ink suitable for use with an inkjet printer is defined by the ability to eject a well-formed single drop without the formation of satellite drops. We propose that a parameter space defined by the dimensionless parameters  $Z$  and  $We_j$  can best determine the printability of a fluid with known (Newtonian) physical properties. The use of  $Z$  is justified because it does not contain a velocity term. The Weber number is determined using the velocity of the fluid prior to drop formation, i.e. the fluid jet Weber number,  $We_j$ . This more accurately captures the mechanisms of drop ejection and gives a fairer representation of the practical utility of an ink. The region of printability is bounded by maximum and minimum values of  $We_j$  ( $2 < We_j < 25$ ) and is shaped in the fashion of a parallelogram, centred around  $Z \approx 2-20$ , with different behavior at low and high values of  $Z$ . The lower bound of  $We_j = 2$  represents the limiting capillarity forces that must be overcome for drop formation (bound I). The upper bound of  $We_j = 25$  represents the intrinsic instability of the extended tail that forms as a drop is ejected (bound III). The low  $Z$  limit to printability (bound II) indicates a region where viscous forces become increasingly important and the minimum  $We_j$  for drop ejection increases with decreasing  $Z$ , accompanied by an increase in the minimum actuation voltage for drop ejection. At large  $Z$ , the maximum  $We_j$  before satellites form decreases with increasing  $Z$  because the low viscosity fluid forms liquid columns that readily pinch off to form satellites (bound IV). However, at both high and low values of  $Z$ , the range of fluid velocities ( $We_j$ ) between the minimum value for drop ejection and the onset for satellite formation is small, and thus the practical range for ink printability is approximately bound by  $2 < Z < 20$ , which is slightly greater than the printability range proposed by Reis and Derby in their initial CFD study<sup>16</sup> and that determined experimentally by Jang *et al.* using squeeze mode drop generators.<sup>22</sup>

## ACKNOWLEDGMENTS

We would like to thank the Engineering and Physical Sciences Research Council (EPSRC) who supported this work through the grant "Challenges in High Resolution Inkjet Printing," reference EP/L012022/1. We also acknowledge the support of the China Science Council and the University of Manchester through the provision of a postgraduate studentship.

## APPENDIX: THE NUMBER $Z$ AND THE PRINTABILITY OF INKS

In the appendix, we give a more complete survey of the range of the dimensionless number  $Z$  for ink/drop generator combinations where successful stable inkjet drop generation has been reported. Table III gives the nozzle manufacturer, mode of fluid actuation, ink composition, actuating waveform, and dimensionless number,  $Z$ , in each case.

TABLE III. A summary of the range of Z number reported for printability using drop-on-demand (DOD) inkjet printheads.

Reference	Nozzle manufacturer	Actuation mode	Nozzle diameter ( $\mu\text{m}$ )	Inks <sup>a</sup>	Waveform type <sup>b</sup>	Z number
Link and Semiat <sup>35</sup>	Aprion	Push	30	Black dye ink	Trapezoidal	2.68
Dong <i>et al.</i> <sup>20</sup>	Trident	Push	53	GWI, GW, and DI water	Single peak and double peak	8.78, 12.6, 62.2
Choi <i>et al.</i> <sup>36</sup>	Self-designed	Push	100	GW	...	0.23-84.77
Rho <i>et al.</i> <sup>37</sup>	Dimatix	Shear	19	NP and pure solvents	...	0.55-36.7
Hill <i>et al.</i> <sup>38</sup>	Dimatix	Shear	21.5	$\alpha$ -Terpineol-based inks	Trapezoidal	3-24
Liu <i>et al.</i> <sup>24</sup>	MicroFab	Squeeze	30	GW	Trapezoidal, double, and bipolar	2.15-46
Tsai <i>et al.</i> <sup>23</sup>	MicroFab	Squeeze	30	EG and alcohol	Bipolar	2.99, 21.23
Tsai <i>et al.</i> <sup>23</sup>	MicroFab	Squeeze	30	Silver nanoparticle suspension and DI water	Bipolar	6.28, 43.48
Wu <i>et al.</i> <sup>39</sup>	MicroFab	Squeeze	40	Computational fluid dynamics	Trapezoidal	17.39-53.7
Gan <i>et al.</i> <sup>40</sup>	MicroFab	Squeeze	50	PEDOT and DI water	Double W-shaped, trapezoidal, and bipolar	1.98, 60.4
Jang <i>et al.</i> <sup>22</sup>	MicroFab	Squeeze	50	Mixtures of EG/DI, DEG <i>et al.</i>	Bipolar	4-14
Jo <i>et al.</i> <sup>41</sup>	MicroFab	Squeeze	50	GW	Trapezoidal	4-41.67
Shield <i>et al.</i> <sup>42</sup>	Self-designed	Squeeze	50	EG and DI water	Trapezoidal	18.4, 64
Shin <i>et al.</i> <sup>43</sup>	Micro drop	Squeeze	50	EG/DI and DI water	Trapezoidal and double	35.5, 105.3
Son <i>et al.</i> <sup>44</sup>	MicroFab	Squeeze	50	DI water	Bipolar	58.80
Tai <i>et al.</i> <sup>45</sup>	MicroFab	Squeeze	50	GW	Trapezoidal	0.67-50
Bienia <i>et al.</i> <sup>46</sup>	Ceradrop	Squeeze	42, 52	Solvents and ceramic suspensions	Trapezoidal	1.27-16.69
Nallan <i>et al.</i> <sup>29</sup>	MicroFab	Squeeze	60	Solvent mixtures and gold nanoparticle suspensions	Bipolar	1-60
Szczzech <i>et al.</i> <sup>47</sup>	MicroFab	Squeeze	60	Nanoparticle suspension	Bipolar	23.1-47.9
Perelaer <i>et al.</i> <sup>25</sup>	Micro drop	Squeeze	70	PT and PB	Trapezoidal	7.92-63.4
Seerden <i>et al.</i> <sup>4</sup>	Sanders design international	Squeeze	70	Alumina/Paraffin suspension	Trapezoidal	2.56-17.75
Reis <i>et al.</i> <sup>28</sup>	Sanders design international	Squeeze	75	Alumina/Paraffin suspension	Trapezoidal	1.48-12.7
de Gans <i>et al.</i> <sup>7</sup>	Micro drop	Squeeze	30-100	Polystyrene nanoparticle inks	Trapezoidal	21-91
Kim and Baek <sup>33</sup>	MicroFab	Squeeze	2000	Computational fluid dynamics	Trapezoidal	1-14
Delrot <i>et al.</i> <sup>48</sup>	Self-designed	Thermal	100-300	Organic dye and GW	...	0.67-100
Esposito <i>et al.</i> <sup>49</sup>	HP Deskjet1000	Thermal	20	Nanoparticle suspension	...	6.73, 10.28

<sup>a</sup>DEG, EG, GW, GWI, NP, PB, PEDOT, and PT denote diethylene glycol, ethylene glycol, glycerol-water mixture, glycerol-water-isopropanol mixture, pre-crystallized NiO nanoparticle ink, polystyrene-butyl acetate mixture, poly(3,4-ethylenedioxythiophene), and polystyrene-toluene mixture, respectively. Paraffin (wax) and PEDOT are non-Newtonian fluids.

<sup>b</sup>The waveforms for inkjet nozzles operated in different modes are a little bit different.

## REFERENCES

- H. Sirringhaus, T. Kawase, R. H. Friend, T. Shimoda, M. Inbasekaran, W. Wu, and E. P. Woo, "High-resolution inkjet printing of all-polymer transistor circuits," *Science* **290**(5499), 2123–2126 (2000).
- S. E. Burns, P. Cain, J. Mills, J. Z. Wang, and H. Sirringhaus, "Inkjet printing of polymer thin-film transistor circuits," *MRS Bull.* **28**(11), 829–834 (2003).
- M. Mott, J. H. Song, and J. R. G. Evans, "Microengineering of ceramics by direct ink-jet printing," *J. Am. Ceram. Soc.* **82**(7), 1653–1658 (1999).
- K. A. M. Seerden, N. Reis, J. R. G. Evans, P. S. Grant, J. W. Halloran, and B. Derby, "Ink-jet printing of wax-based alumina suspensions," *J. Am. Ceram. Soc.* **84**(11), 2514–2520 (2001).
- B. Derby, "Inkjet printing ceramics: From drops to solid," *J. Eur. Ceram. Soc.* **31**(14), 2543–2550 (2011).

- <sup>6</sup>R. E. Saunders and B. Derby, "Inkjet printing biomaterials for tissue engineering: Bioprinting," *Int. Mater. Rev.* **59**(8), 430–448 (2014).
- <sup>7</sup>B. J. de Gans, P. C. Duineveld, and U. S. Schubert, "Inkjet printing of polymers: State of the art and future developments," *Adv. Mater.* **16**(3), 203–213 (2004).
- <sup>8</sup>T. M. Wang, M. A. Roberts, I. A. Kinloch, and B. Derby, "Inkjet printed carbon nanotube networks: The influence of drop spacing and drying on electrical properties," *J. Phys. D: Appl. Phys.* **45**, 315304 (2012).
- <sup>9</sup>F. Torrisi, T. Hasan, W. P. Wu, Z. P. Sun, A. Lombardo, T. S. Kulmala, G. W. Hsieh, S. J. Jung, F. Bonaccorso, P. J. Paul, D. P. Chu, and A. C. Ferrari, "Inkjet-printed graphene electronics," *ACS Nano* **6**(4), 2992–3006 (2012).
- <sup>10</sup>P. He and B. Derby, "Inkjet printing ultra-large graphene oxide flakes," *2D Mater.* **4**, 021021 (2017).
- <sup>11</sup>G. D. Martin, S. D. Hoath, and I. M. Hutchings, "Inkjet printing—The physics of manipulating liquid jets and drops," *J. Phys.: Conf. Ser.* **105**, 012001 (2008).
- <sup>12</sup>B. Derby, "Inkjet printing of functional and structural materials: Fluid property requirements, feature stability, and resolution," *Annu. Rev. Mater. Res.* **40**, 395–414 (2010).
- <sup>13</sup>O. A. Basaran, H. J. Gao, and P. P. Bhat, "Non-standard inkjets," *Annu. Rev. Fluid Mech.* **45**, 85–113 (2013).
- <sup>14</sup>J. E. Fromm, "Numerical-calculation of the fluid-dynamics of drop-on-demand jets," *IBM J. Res. Dev.* **28**(3), 322–333 (1984).
- <sup>15</sup>J. F. Dijkman, "Hydrodynamics of small tubular pumps," *J. Fluid Mech.* **139**, 173–191 (1984).
- <sup>16</sup>N. Reis and B. Derby, "Ink jet deposition of ceramic suspensions: Modelling and experiments of droplet formation," in *Solid Freeform and Additive Fabrication*, MRS Symposium Proceedings (Materials Research Society, Warrendale, PA, USA, 2000), Vol. 625, pp. 117–122.
- <sup>17</sup>P. C. Duineveld, M. A. de Kok, M. Buechel, A. H. Sempel, K. A. H. Mutsaers, P. van de Weijer, I. G. J. Camps, T. J. M. van den Biggelaar, J. Rubingh, and E. I. Haskal, "Ink-jet printing of polymer light-emitting devices," *Proc. SPIE* **4464**, 59–67 (2001).
- <sup>18</sup>Q. Xu and O. A. Basaran, "Computational analysis of drop-on-demand drop formation," *Phys. Fluids* **19**, 102111 (2007).
- <sup>19</sup>X. Mao, L. Zhang, Z. Zhao, and F. Lin, "Generation of droplets via oscillations of a tapered capillary tube filled with low-viscosity liquids," *Phys. Fluids* **29**, 067104 (2017).
- <sup>20</sup>H. M. Dong, W. W. Carr, and J. F. Morris, "An experimental study of drop-on-demand drop formation," *Phys. Fluids* **18**, 072102 (2006).
- <sup>21</sup>P. K. Notz and O. A. Basaran, "Dynamics and breakup of a contracting liquid filament," *J. Fluid Mech.* **512**, 223–256 (2004).
- <sup>22</sup>D. Jang, D. Kim, and J. Moon, "Influence of fluid physical properties on ink-jet printability," *Langmuir* **25**(5), 2629–2635 (2009).
- <sup>23</sup>M. H. Tsai, W. S. Hwang, H. H. Chou, and P. H. Hsieh, "Effects of pulse voltage on inkjet printing of a silver nanopowder suspension," *Nanotechnology* **19**, 335304 (2008).
- <sup>24</sup>Y. F. Liu, M. H. Tsai, Y. F. Pai, and W. S. Hwang, "Control of droplet formation by operating waveform for inks with various viscosities in piezoelectric inkjet printing," *Appl. Phys. A: Mater. Sci. Process.* **111**(2), 509–516 (2013).
- <sup>25</sup>J. Perelaer, P. J. Smith, M. M. P. Wijnen, E. van den Bosch, R. Eckardt, P. Ketelaars, and U. S. Schubert, "Droplet tailoring using evaporative inkjet printing," *Macromol. Chem. Phys.* **210**(5), 387–393 (2009).
- <sup>26</sup>D. Y. Shin, P. Grassia, and B. Derby, "Numerical and experimental comparisons of mass transport rate in piezoelectric drop-on-demand print head," *Int. J. Mech. Sci.* **46**(2), 181–199 (2004).
- <sup>27</sup>J. R. Castrejon-Pita, N. F. Morrison, O. G. Harlen, G. D. Martin, and I. M. Hutchings, "Experiments and Lagrangian simulations on the formation of droplets in drop-on-demand mode," *Phys. Rev. E* **83**, 036306 (2011).
- <sup>28</sup>N. Reis, C. Ainsley, and B. Derby, "Ink-jet delivery of particle suspensions by piezoelectric droplet ejectors," *J. Appl. Phys.* **97**, 094903 (2005).
- <sup>29</sup>H. C. Nallan, J. A. Sadie, R. Kitsomboonloha, S. K. Volkman, and V. Subramanian, "Systematic design of jettable nanoparticle-based inkjet inks: Rheology, acoustics, and jettability," *Langmuir* **30**(44), 13470–13477 (2014).
- <sup>30</sup>T. Driessen and R. Jeurissen, "Drop formation in inkjet printing," in *Fundamentals of Inkjet Printing*, edited by S. D. Hoath (Wiley VCH, Weinheim, Germany, 2016), pp. 93–115.
- <sup>31</sup>B. Derby and N. Reis, "Inkjet printing of highly loaded particulate suspensions," *MRS Bull.* **28**(11), 815–818 (2003).
- <sup>32</sup>R. Schulkes, "The contraction of liquid filaments," *J. Fluid Mech.* **309**, 277–300 (1996).
- <sup>33</sup>E. Kim and J. Baek, "Numerical study on the effects of non-dimensional parameters on drop-on-demand droplet formation dynamics and printability range in the up-scaled model," *Phys. Fluids* **24**, 082103 (2012).
- <sup>34</sup>K.-S. Kwon, "Experimental analysis of waveform effects on satellite and ligament behavior via *in situ* measurement of the drop-on-demand drop formation curve and the instantaneous jetting speed curve," *J. Micromech. Microeng.* **20**, 115005 (2010).
- <sup>35</sup>N. Link and R. Semiat, "Ink drop motion in wide-format printers," *Chem. Eng. Process.* **48**(1), 68–83 (2009).
- <sup>36</sup>I. H. Choi, Y. K. Kim, S. Lee, S. H. Lee, and J. Kim, "Pneumatic drop-on-demand printing system with an extended printable liquid range," *J. Microelectromech. Syst.* **24**(4), 768–770 (2015).
- <sup>37</sup>Y. Rho, K. Y. Kang, and D. Lee, "Highly crystalline Ni/NiO hybrid electrodes processed by inkjet printing and laser-induced reductive sintering under ambient conditions," *Nanoscale* **8**(16), 8976–8985 (2016).
- <sup>38</sup>T. Hill, T. L. Reitz, M. A. Rottmayer, and H. Huang, "Controlling inkjet fluid kinematics to achieve SOFC cathode micropatterns," *ECS J. Solid State Sci. Technol.* **4**(4), P3015–P3019 (2015).
- <sup>39</sup>H. C. Wu, W. S. Hwang, and H. J. Lin, "Development of a three-dimensional simulation system for micro-inkjet and its experimental verification," *Mater. Sci. Eng., A* **373**(1–2), 268–278 (2004).
- <sup>40</sup>H. Y. Gan, X. C. Shan, T. Eriksson, B. K. Lok, and Y. C. Lam, "Reduction of droplet volume by controlling actuating waveforms in inkjet printing for micro-pattern formatio," *J. Micromech. Microeng.* **19**(5), 055010 (2009).
- <sup>41</sup>B. W. Jo, A. Lee, K. H. Ahn, and S. J. Lee, "Evaluation of jet performance in drop-on-demand (DOD) inkjet printing," *Korean J. Chem. Eng.* **26**(2), 339–348 (2009).
- <sup>42</sup>T. W. Shield, D. B. Bogy, and F. E. Talke, "Drop formation by DOD ink-jet nozzles: A comparison of experiment and numerical simulation," *IBM J. Res. Dev.* **31**(1), 96–110 (1987).
- <sup>43</sup>P. Shin, J. Sung, and M. H. Lee, "Control of droplet formation for low viscosity fluid by double waveforms applied to a piezoelectric inkjet nozzle," *Microelectron. Reliab.* **51**(4), 797–804 (2011).
- <sup>44</sup>Y. Son, C. Kim, D. H. Yang, and D. J. Ahn, "Spreading of an inkjet droplet on a solid surface with a controlled contact angle at low Weber and Reynolds numbers," *Langmuir* **24**(6), 2900–2907 (2008).
- <sup>45</sup>J. Tai, H. Y. Gan, Y. N. Liang, and B. K. Lok, "Control of droplet formation in inkjet printing using Ohnesorge number category: Materials and processes," in *10th Electronics Packaging Technology Conference (IEEE, 2008)*, pp. 761–766.
- <sup>46</sup>M. Bienia, M. Lejeune, M. Chambon, V. Baco-Carles, C. Dossou-Yovo, R. Noguera, and F. Rossignol, "Inkjet printing of ceramic colloidal suspensions: Filament growth and breakup," *Chem. Eng. Sci.* **149**, 1–13 (2016).
- <sup>47</sup>J. B. Szczech, C. M. Megaridis, D. R. Gamota, and J. Zhang, "Fine-line conductor manufacturing using drop-on-demand PZT printing technology," *IEEE Trans. Electron. Packag. Manuf.* **25**(1), 26–33 (2002).
- <sup>48</sup>P. Delrot, M. A. Modestino, F. Gallaire, D. Psaltis, and C. Moser, "Inkjet printing of viscous monodisperse microdroplets by laser-induced flow focusing," *Phys. Rev. Appl.* **6**, 024003 (2016).
- <sup>49</sup>V. Esposito, C. Gadea, J. Hjelm, D. Marani, Q. Hu, K. Agersted, S. Ramousse, and S. H. Jensen, "Fabrication of thin yttria-stabilized-zirconia dense electrolyte layers by inkjet printing for high performing solid oxide fuel cells," *J. Power Sources* **273**, 89–95 (2015).